Fluid Phase Equilibria, 80 (1992) 305–321
Elsevier Science Publishers B.V., Amsterdam

Measurement of Thermal Diffusivity of the Refrigerants R22 and R134a by means of Dynamic Light Scattering

B. Kruppa, J. Straub

Lehrstuhl A für Thermodynamik, Technische Universität München, P.O. Box 202420, 8000 München 2, Federal Republic of Germany

Keywords: thermal diffusivity, dynamic light scattering, alternative Refrigerants

ABSTRACT

Dynamic light scattering is an efficient method of determining thermal diffusivity of transparent fluids in a wide region of state, its main advantage over conventional methods being the fact of thermodynamic equilibrium within the sample. This paper presents new thermal diffusivity measurements of the environmentally acceptable refrigerants R22 and R134a, the latter substance being a possible substitute for the refrigerant R12. Measurements were carried out along the critical isochore, both coexisting phases and up to seven isotherms within a range of state characterized in terms of reduced pressure and density as $0.5 < p/p_c < 3.0$ and $0.2 < \varrho/\varrho_c < 2.3$ respectively, amounting to a total of 300 measurement points per substance. Provided an equation of state to determine c_p, the diffusivity data can also be expressed in terms of thermal conductivity λ.

INTRODUCTION

In the field of heat transfer and energy conversion, particularly in processes operating under thermodynamic cycles, a knowledge of the thermodynamic properties of the working fluid is of vital interest, not only for understanding the process itself, but also for planning and designing the appropriate components. The substance water, the primary working fluid for energy processes, has been sufficiently investigated with respect to its thermal, caloric and transport properties.

However, with low and mediate temperature cyclic processes such as the Organic Rankine Cycle, heatpumps and refrigeration processes, there is still a lack of thermophysical data of the appropriate fluids, particularly in the

0378-3812/92/$05.00

area of transport properties. This is due to the fact that transport properties such as thermal conductivity, diffusivity and viscosity are generally difficult to measure and are burdened with uncertainties typically an order of magnitude greater than their corresponding equilibrium properties (such as p, ϱ,T -measurements). This can be shown quite clearly in the current search for environmentally acceptable substitutes for the chlorofluorocarbons typically used in those processes and being to a great extent responsible for the destruction of the stratospheric ozone-layer. While, after some three years of research, the equilibrium p,ϱ,T -properties of the most promising alternatives CH_2FCF_3 (R134a) and $CHCl_2CF_3$ (R123) have been investigated sufficiently to allow for the development of tables and equations, the amount of reliable measurement data on transport properties is far less and not nearly as evenly distributed, with some regions of state totally lacking measurements.

For calculations involving heat transfer, it is the knowledge of the transport properties that constitutes a necessary information for designing and dimensioning components, the properties appearing often in the dimensionless numbers as Nusselt, Reynolds, Prandtl, Grashof and Rayleigh.

In this paper, our thermal diffusivity measurements of the alternative refrigerants R22 and R134a obtained by light scattering are presented. Provided a good equation of state for ϱ and c_p, thermal conductivity can be calculated from the diffusivity data as will be shown for the substance R22. Our measurements also cover the critical region, where conventional stationary and instationary methods for determining λ are subject to large errors due to convective effects and are hence particularly scarce. Here, dynamic light scattering can also be used as an accurate method to determine λ.

METHOD OF MEASUREMENT

Dynamic light scattering represents a non-invasive optical technique for measuring thermal diffusivity. The fluid under investigation is kept in thermal equilibrium with no internal sources of heat or macroscopic temperature gradients present, which is a significant advantage over the conventional techniques of determining transport properties such as the parallel plate or hot wire methods. The information on thermal diffusivity is obtained by investigating the relaxation behaviour of microscopic thermodynamic fluctuations. Since the method is intrinsically absolute in nature, there is no need for calibration or for introducing corrective terms. According to the optical arrangement for detecting the scattered light, measurements can be made in the fluid region (heterodyne detection) and in the extended critical region (homodyne detection) with an accuracy typically under 2% depending on the investigated region of state. At lower fluid densities (below 100 kg/m^3) the scattered intensities are too low to be evaluated accurately, and thus limit the range of application. For an explicit treatment of dynamic light scattering and its applications we refer to such standard literature as Berne & Pecora (1976) and Chu (1974).

The experimental apparatus used in our investigations has been described in detail by Reile (1984) and Jany (1987). An argon-ion laser with a maximum power output of 300 mW is focussed into a test cell. The light scattered by the microscopic temperature fluctuations is recorded at variable scattering angles (3° – 15°) by a photomultiplier. This signal is then fed into a digital correlator which builds the correlation function g(t), the statistical average behaviour of the dissipative fluctuations. A regressional analysis yields the characteristic decay-time t_c of this exponential function from which thermal diffusivity can directly be calculated.

On account of the relatively high critical temperatures of the alternative refrigerants, we have developed an electronically regulated test cell capable of sustaining a long term temperature stability (± 2 mK over 24 h) at temperatures up to 500 K (Kruppa 1988). This stability is important when measuring in the critical region where **a** decreases over several orders of magnitude and where macroscopic temperature stability not only limits the possible approach to the critical point but also represents an increasing source of error in the determination of **a**. In this investigation we have been able to measure thermal diffusivites to within 0.01 K of the critical point. While the above-mentioned temperature stability would allow for closer approaches, other limiting factors such as multiple scattering, gravitation, laser heating or limits of the hydrodynamic region become a major source of error in this region.

In the extended critical region, measurements were made using the homodyne method of light scattering. The scattered light $\bar{I}_S$ is directly measured by the photomultiplier at angles Θ between 8° – 10°. Light scattered off the cell windous I_0 (representing a local oscillator) is effectively screened out of the detection by means of a pinhole situated in front of the cell windows, ensuring the criterion $\bar{I}_S \gg I_0$ for the evaluation of the correlation function by a single exponental.

In the fluid region, where scattered light intensities are small, the heterodyne method was employed. Here signal enhancement is achieved by superimposing a local oscillator, the light I_0 scattered off the cell windows, with $\bar{I}_S$. By measuring at small scattering angles (Θ between 3° – 5°) and shifting the scattering volume with respect to the window surface, the assumption $I_0 \gg \bar{I}_S$ can be assured.

RESULTS

The objective behind this investigation was a systematic coverage of a broad region of state within the limits set by the applicability of the method or the apparatus. For this reason, thermal diffusivity measurements were made along four super- and up to three subcritical isotherms $\tau = \pm 10^{-3}, \pm 10^{-2}$, $\pm 5 \cdot 10^{-2}$ and $+10^{-1}$, where τ denotes the reduced temperature and is characterized by $\tau = (T - T_c)/T_c$. Measurements were also made along the critical isochore as well as both coexisting phases. On average, 35 measurement points were taken along each path. The covered region of state expressed in terms

of density and pressure is approximately 100 kg/m^3 < ρ < 1200 kg/m^3 and 290 K < T < 420 K. While the measurements at higher temperatures and pressures were restricted by the pressure resistance of the quartz cell windows, those obtained in the low density region were limited by the applicability of the method due to low light scattering intensities.

In addition to thermal diffusivity, the temperature, pressure and refractive index of the substances were also measured. Using the Lorentz - Lorenz relation, density values can be calculated from the refractive index measurements. Figures 1 to 4 depict the measured values of thermal diffusivity of the substances R22 and R134a. Figures 1 and 3 plot **a** against the reduced temperature in double logarithmic axes for both phases of the coexistence curve and for the critical isochore. The logarithmic presentations in Figures 2 and 4 depict **a** vs. the reduced density ϱ/ϱ_c for the coexistence curve and seven isotherms.

ACCURACIES

Thermal diffusivity

Since dynamic light scattering represents a statistical process, the measurements of diffusivities are invariably subject to statistical deviation in addition to experimental errors. In the following we will briefly classify the main sources of error. The equation determining thermal diffusivity can be expressed as:

$$\mathbf{a} = \frac{1}{t_c \, \vec{q}^{\,2}} \tag{1}$$

where $\vec{q}$ is the scattering vector and defines the scattering geometry

$$|\vec{q}| = q = \frac{4\pi n}{\lambda_L} sin\left(\frac{\Theta}{2}\right). \tag{2}$$

Here n is the refractive index of the fluid, λ_L the wavelength of the incident light and Θ the scattering angle. Errors made in the determination of $\vec{q}$ can easily be assesed.

λ_L - The error in the wavelength of the incident light can be neglected, as the use of a frequency stabilizing etalon reduces this error to the order of 10^{-3}%.

n - Aside from its direct influence on **a**, refractive index errors also affect the determination of the scattering angle Θ due to the optical geometry. However, both errors have a compensating effect, such that a deviation $\Delta n/n$ of 10% only contributes to an error in $\Delta \mathbf{a}/\mathbf{a}$ of 0.3%. Thus n-measurements need not necessarily be made. In our experiments the

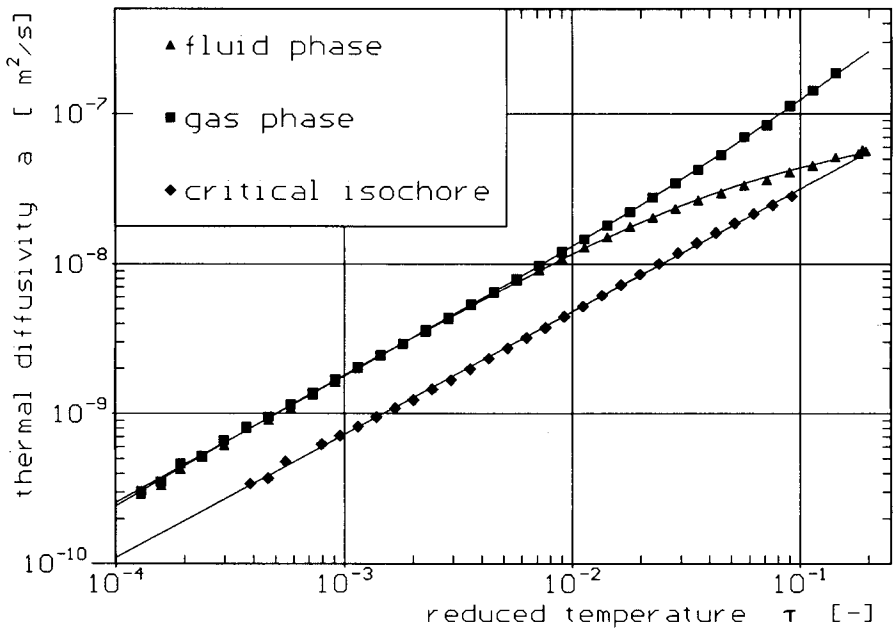

Fig.1 Thermal diffusivity of R22 along the two-phase region and critical isochore

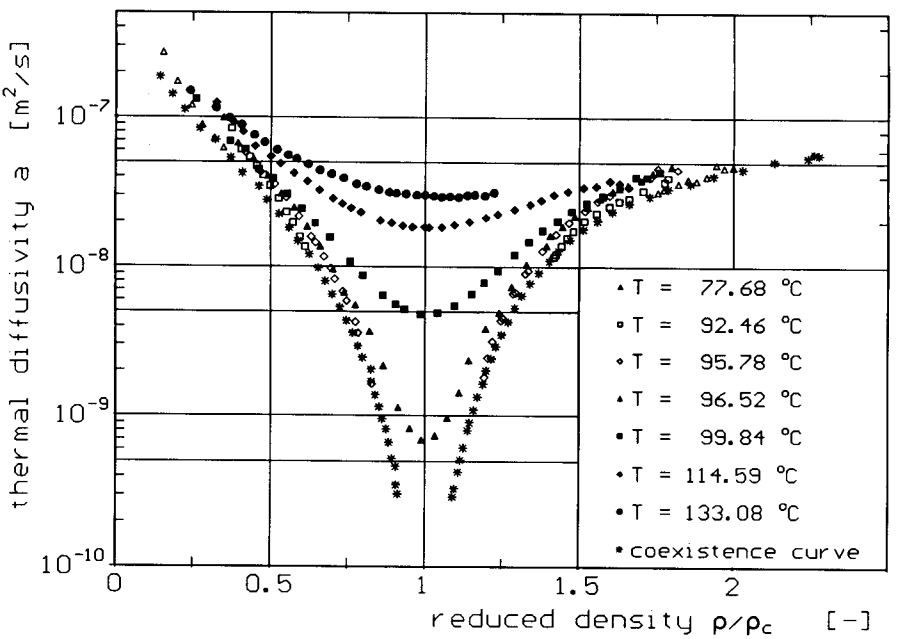

Fig.2 Thermal diffusivity of R22 along isotherms

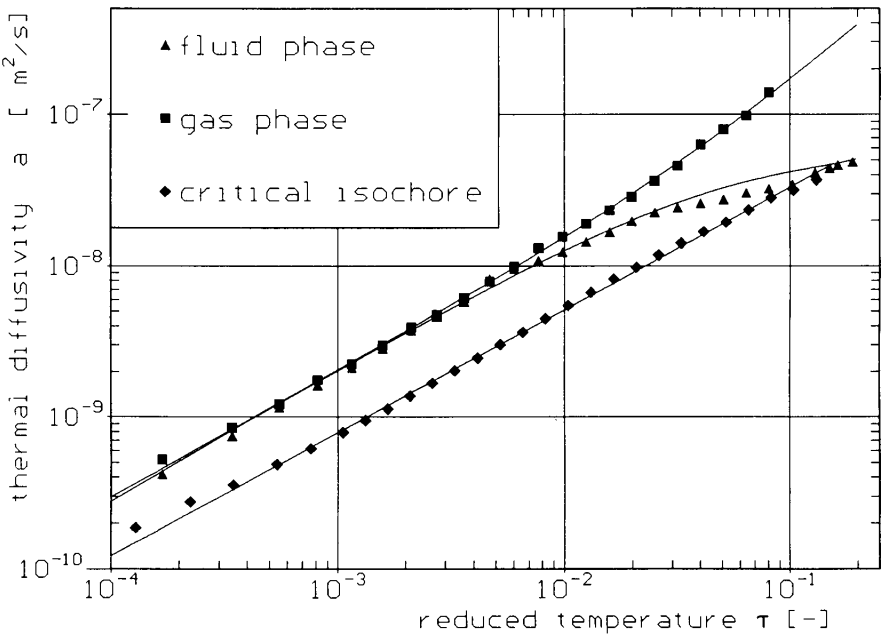

Fig.3 Thermal diffusivity of R134a along the two-phase region and critical isochore

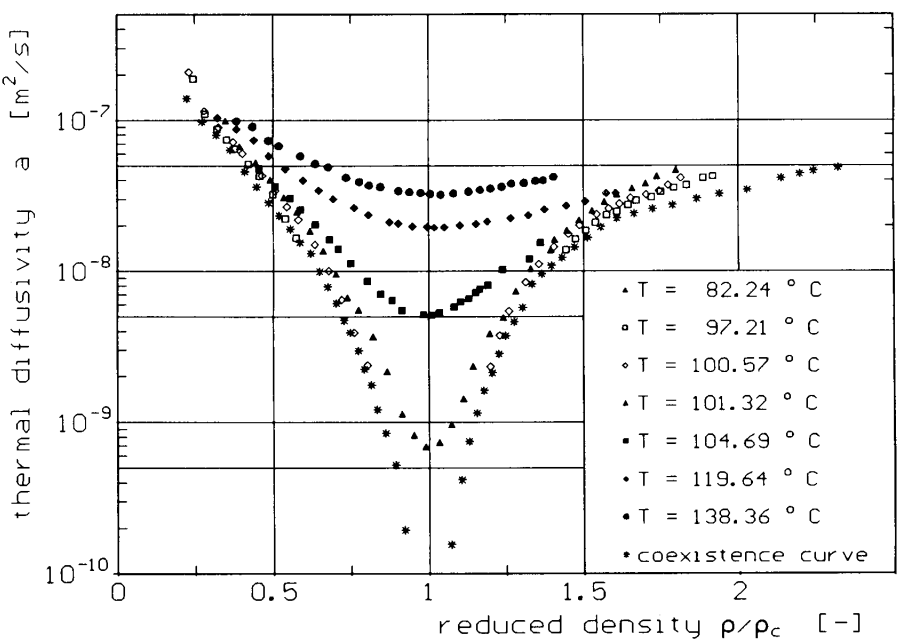

Fig.4 Thermal diffusivity of R134a along isotherms

refractive index is determined with an accuracy of $\Delta n < 5 \cdot 10^{-4}$. The resulting error of Δn on $\Delta \mathbf{a}/\mathbf{a}$ is of the order 0.08%.

Θ - The scattering angle must be carefully measured. In our apparatus, Θ is measured with an accuracy $\Delta\Theta < 6$"using a high precision dividing head. Thus, its overall effect on $\Delta \mathbf{a}/\mathbf{a} < 0.05\%$ is relatively small.

t_c - The main source of error lies in the determination of the decay time t_c through digital correlation due to the statistical process involved. A detailed treatment of the statistical accuracy in light scattering experiments, including such error sources as afterpulse and dead-time effects of the detection system, bias, optimizing experimental parameters (such as photon counts/sampletime, sampletime/decaytime, runtime ect.) can be found in Jakeman (1971) and Degiorgio (1971).

Perhaps the single largest error in light scattering experiments arises from an undesired influence of both measurement methods known as partial heterodyning or homodyning. If the afore-mentioned assumptions $\bar{I}_S \gg I_0$ or $I_0 \gg \bar{I}_S$ are not satisfied in homodyne or heterodyne experiments respectively, the correlation function, which is fitted to a single exponential is contaminated by the addition of a second exponential, the decay times differing by a factor 2. An I_0 contribution of 0.5% in homodyne experiments can already account for errors in the determination of $\mathbf{a}$ of the order of 1% (Wu 1988). $\bar{I}_S/I_0$ can be estimated from the correlated data, or obtained directly by experiment (evacuating the test cell keeping all other parameters constant). In homodyne experiments, this source of error becomes increasingly noticeable at further distances from the critical point, where low light scattering signals and a corresponding high laser power increases the contribution of I_0. We have been able to keep the influence of this error source on $\mathbf{a}$ under 1% in most cases.

In the immediate critical region the geometry of the test cell and that of the optical setup increasingly influences the accuracy of diffusivity measurements. Gravitation, multiple scattering, limits of the hydrodynamic region and laser heating are the main sources of error and have been treated in Kruppa (1988). The gravitational effect on $\mathbf{a}$ is briefly demonstrated here. By measuring thermal diffusivity over the height of the test cell, the influence of the density profile induced by gravity on $\mathbf{a}$ can be measured.

Figure 5 depicts the $\mathbf{a}$ measurements over a 12mm height span of the test cell for the substance R134a at near-critical density. $T - T_c$ was 40mK corresponding to a τ of 10^{-4}. The height at 0 mm corresponds to critical density. The measurements were made 12 hours after equilibration, allowing sufficient time for the complete formation of the density gradient. As can be seen from the figure, diffusivity is significantly influenced by the height. An exact determination of the position of critical density within the test cell is necessary ($\pm$0.2mm in our experiments) if such errors are to be minimized.

The overall accuracy of our thermal diffusivity measurements lies between 0.5 - 2%, those obtained in the critical region being more accurate than measurements made in regions of low light scattering intensities.

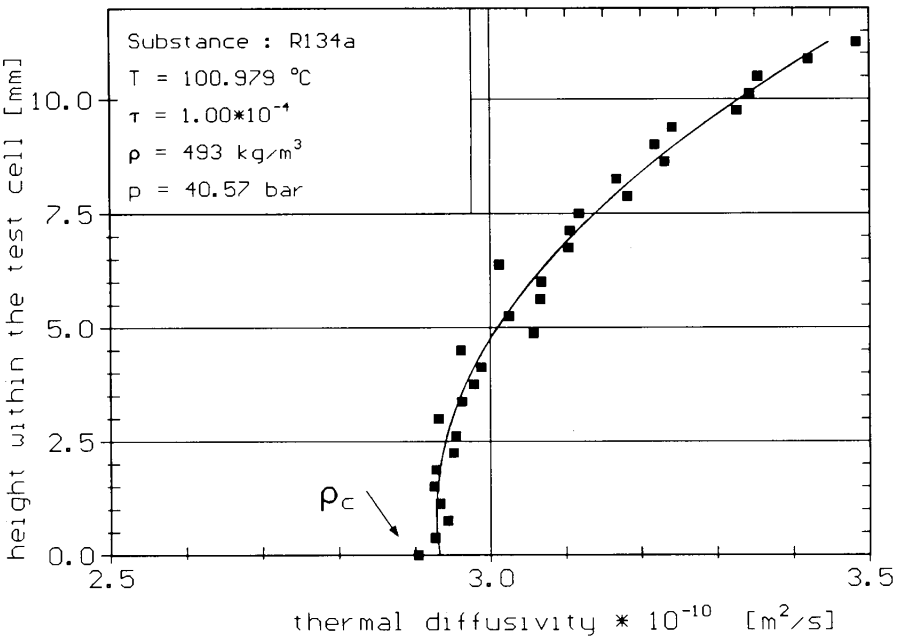

Fig.5 Gravitaional influence on thermal diffusivity near the critical point

p,ϱ,T - Data

T - The fluid temperature was measured with a low-drift platinum resistance thermometer (PT 100) with a resolution under 1mK. Calibration resulted in a maximum absolute temperature deviation of 20mK between 50 - 150 °C. A repeated measurement of the critical temperature of R22 within two years revealed negligible drift.

p - A piezoresistive pressure transducer was used for measurements. Here calibration over 15 MPa resulted in a maximum deviation of $5 \cdot 10^{-3}$ MPa while the resolution was under $1 \cdot 10^{-4}$ MPa.

ϱ - Density was calculated from the refractive index data using the Lorentz-Lorenz relation. With $\Delta n = 5 \cdot 10^{-4}$, the resulting accuracy in the density measurements is 0.3%. A comparison of our measured R22 densities with an equation of state from Wagner(1989) yields maximum deviations of 0.7%.

EVALUATION

Critical values

Measurements made along the coexistence curve and the critical isochore closely approach the critical point, enabling the determination of critical parameters. Critical temperature T_c is determined by an optical method and

by the evaluation of the refractive index data, the latter method being the more precise. The refractive index measurements also yield values for n_c and, assuming ϱ_c from the literature, the Lorentz-Lorenz constant LL_c. Table 1 lists the critical values for the substances R22 and R134a.

TABLE 1

Critical values

	T_c [K]	n_c [−]	p_c [MPa]	ϱ_c [kgm^{-3}]	LL_c [m^{3}kmol^{-1}]
R22	369.29	1.1109	4.965	520.0 |1|	11.846
R134a	374.09	1.0885	4.030	512.2 |2|	10.427

| 1 | : Wagner(1989), | 2 | : Basu(1988)

While the T_c and p_c values for R22 are in good agreement with those of other authors (Japanese Association of Refrigeration 1975), the values for R134a are lower than those reported by Basu(1988), McLinden(1989) and Kubota(1989).

Thermal diffusivity

In the following we list only the evaluations of the measurements along the coexistence curve and the critical isochore, as we are still working on a more general evaluation of thermal diffusivity along isotherms for different substances. When plotted in double logarithmic form along reduced temperature, the values of **a** appear as a straight line in the critical region and can be described by a simple power law which is also in accordance with scaling theory

$$\mathbf{a} = a_0 \tau^{\mu}. \tag{3}$$

This equation can be used to describe thermal diffusivity along the critical isochore in the entire investigated region. However, in the fluid and gas phases, the measurements deviate off the straight line at further distances from the critical point. As expected, the fluid phase levels out to a linear behaviour while measurements along the gas phase increase, reflecting ideal gas behaviour. With the addition of a temperature dependent term in the exponent, this behaviour can be accounted for

$$\mathbf{a} = a_0 \mid \tau \mid^{\mu_0 + \mu_1 \mid \tau \mid}. \tag{4}$$

Table 2 lists the coefficients and relative standard deviations (SD) obtained by regressional analysis along the respective paths for the two refrigerants.

TABLE 2

Coefficients and relative standard deviations resulting from a fit to Equations 3 and 4

	critical isochore			fluid phase				gas phase			
	a_0 $[10^{-7}]$	μ	SD [%]	a_0 $[10^{-7}]$	μ_0	μ_1	SD [%]	a_0 $[10^{-7}]$	μ_0	μ_1	SD [%]
R22	2.101	0.820	3.0	8.244	0.885	3.88	2.5	5.771	0.838	-1.73	2.5
R134a	2.140	0.811	4.8	8.904	0.880	4.89	7.4	6.231	0.830	-2.71	3.5

The exponents μ and μ_0 are larger than the theoretical value $\nu = 0.63$ from scaling theory. A regional fit of our data by approaching the critical point shows no indication of these values to decrease. The data can also be fitted by an expansion

$$\mathbf{a} = a_0 \mid \tau \mid^{\mu} (1 + a_1\tau^{\Delta} + a_2\tau^{2\Delta}.....) \tag{5}$$

in analogy with the *corrections to scaling* (Wegner 1972) taking into account the extended region around the critical point, with Δ being a correction exponent. However, the initial values for μ and Δ have to be kept within strict boundaries close to the expected theoretical values, and standard deviations of the fit double. If the critical exponent is determined according to its original definition

$$\mu = \lim_{\tau \to 0} \frac{d\, ln(\mathbf{a})}{d\, ln(\tau)}, \tag{6}$$

then the values in table 2 are more reliable than the theoretical one.

Thermal conductivity

Thermal conductivity can be calculated from the diffusivity data using the equation $\mathbf{a} = \lambda/\rho c_p$, provided a good equation for the Helmholtz free energy or an equation of state with an appropriate value of c_{p0} is available, allowing for the determination of ρ and c_p from the T,p-data.
Figure 6 shows λ of the refrigerant R22 as calculated from our thermal diffusivity data along 4 supercritical isotherms and the 2 phase region. The values of c_p were obtained by an equation for the free Helmholtz energy developed by Wagner (1989), while ϱ was calculated from our refractive index measurements. Measurements obtained by Makita (1981) with the concentric cylinder

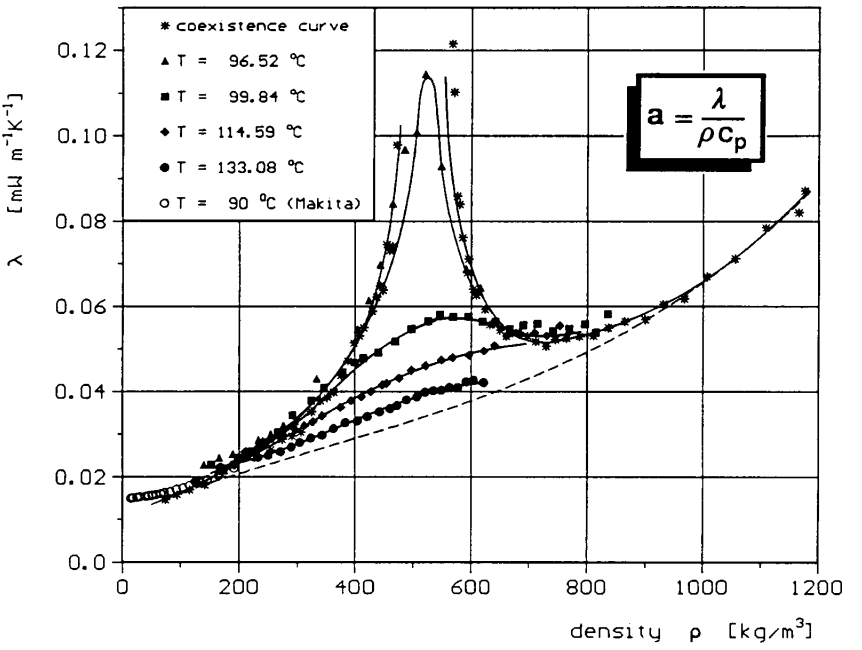

Fig.6 Thermal conductivity of R22

apparatus are also included. While the agreement at distances further from the critical point is very good (90 °C), large differences are observed in the critical region, the values of Makita being larger than those measured by light scattering. This may be due to convective effects in the concentric cylinder apparatus.

CONCLUSIONS

Light scattering measurements of thermal diffusivity of the alternative refrigerants R22 and R134a have been presented, proving this method to be an effective means of measuring this transport property in a broad region of state characterized by 100 kg/m^3 $< \varrho <$ 1200 kg/m^3. By combining the techniques of homodyne and heterodyne detection, measurements can be made up to pressures and temperatures usually limited by constraints imposed by the test cell. In the gas region at lower densities, dynamic light scattering is subject to increasing errors due to low scattering intensites and thus cannot be applied. The accuracy of the light scattering measurements varies between 0.5 and 2.0% depending on the investigated region of state. Measurements along the critical isochore and the coexistence curve can be described by power laws within an error of 7%, the values of the exponents being consistenty higher than expected by scaling theory. Dynamic light scattering can also serve as a complementary technique for determining thermal conductivity, particulary in the critical region where conventional methods are subject to error. We hope

this work serves as a contribution for a better coverage of thermophysical property data of the new environmentally acceptable refrigerants. Our continuing efforts will lie in the investigation of the refrigerants R123a, R142b and R152a as well as mixtures between these substances.

ACKNOWLEDGEMENTS

The authors would like to express their gratitude to the Deutsche Forschungsgemeinschaft (DFG) for supporting this research project and to Daikin Industries Ltd. for providing the refrigerant R134a.

REFERENCES

Basu, R.S., Wilson, D.P., 1989. Thermophysical Properties of 1,1,1,2 - Tetrafluoroethane (R134a). Int. J. of Thermophys., 10: 591-604.
Berne, B.J., Pecora, R., 1976. *Dynamic Light Scattering.* John Whiley, New York.
Chu, B., 1974. *Laser Light Scattering.* Academic Press, New York.
Degiorgio, V., Lastovka, L.B., 1971. Intensity Correlation Spectroscopy. Phys. Rev. A, 4: 2033.
Jakeman, E., Pike, E.R., Swain, S., 1971. Statistical accuracy in the digital autocorrelation of photon counting fluctuations. J. Phys A: Gen. Phys., 4: 517.
Jany, P., Straub, J., 1987. Thermal diffusivity of fluids in a broad region around the critical point. Int. J. of Thermophys., 8: 165-180.
Japanese Association of Refrigeration, 1975. *Thermophysical Properties of Refrigerants R22.* Tokyo.
Kruppa, B., Straub, J., 1988. Experimental apparatus for measuring the thermal diffusivity of pure fluids at high temperatures. Int. J. of Thermophys., 9: 911-922.
Kubota, H., Yamashita, T., Tanaka, Y., Makita, T., 1989. Vapor pressures of new fluorocarbons. Int. J. of Thermophs., 10: 629-638.
Makita, T., Tanaka, Y., Morimoto, Y., Noguchi, M., Kubota, H., 1981. Thermal conductivity of gaseous fluorocarbon refrigerants R12,R13,R22 and R23 under pressure. Int. J. of Thermophys., 2: 249-268.
McLinden, M.O., Gallagher, J.S., Weber, L.A., 1990. ASHRAE Trans., 96.
Reile, E., Jany, P., Straub, J., 1984. Messung der Temperaturleitfähigkeit reiner Fluide und binärer Gemische mit Hilfe der dynamischen Lichtstreuung. Wärme- und Stoffübertragung, 18: 99-108.
Wagner, W., 1989. *private communications.* Ruhr Universität Bochum, FRG.
Wegner, F.J., 1972. Corrections to scaling laws. Phys. Rev. B, 5: 4529-4536.
Wu, G., Fiebig, M., Leipertz, A., 1988. Thermal diffusivity of transparent liquids by photon correlation spectroscopy. Int. J. Heat Mass. Trans., 31: 2555-2558.

Appendix: Measurement Data

R22 isotherms			
T $[K]$	p $[MPa]$	ϱ $[kg/m^3]$	$\mathbf{a} \cdot 10^{-9}$ $[m^2/s]$
350.83	10.35	1039.5	46.969
350.83	9.06	1024.6	46.197
350.83	5.22	963.4	38.698
350.83	4.58	947.4	36.295
350.83	3.48	912.8	31.931
350.83	3.37	165.6	72.793
350.83	2.95	127.3	120.223
350.83	2.61	103.2	173.111
350.83	2.21	79.8	270.342
365.63	8.59	930.1	39.584
365.63	6.87	888.2	32.593
365.62	5.82	847.9	27.481
365.63	5.21	809.7	22.991
365.62	4.82	770.4	17.442
365.63	4.67	740.4	12.139
365.61	4.65	309.3	15.825
365.61	4.58	286.9	23.155
365.62	4.48	258.8	34.794
365.62	4.36	237.3	46.969
365.62	4.18	210.5	60.619
365.62	4.03	194.3	84.363
368.93	10.86	946.1	44.925
368.93	8.29	900.3	39.957
368.93	7.06	863.6	34.431
368.93	5.97	811.0	27.676
368.93	5.44	763.1	19.843
368.93	5.18	717.7	12.853
368.93	5.08	672.9	6.758
368.93	5.05	626.0	2.452
368.93	5.04	407.6	3.613
368.93	5.02	368.0	8.271
368.92	4.96	328.3	15.863
368.93	4.90	307.9	21.690
368.93	4.83	286.5	29.117
368.93	4.63	243.1	42.819
368.93	4.45	218.7	57.977
369.67	10.28	935.9	46.982

R22 isotherms			
T $[K]$	p $[MPa]$	ϱ $[kg/m^3]$	$\mathbf{a} \cdot 10^{-9}$ $[m^2/s]$
369.67	7.97	885.1	38.225
369.67	6.61	836.7	32.348
369.68	5.81	794.8	25.233
369.67	5.39	752.2	18.680
369.66	5.19	724.9	13.864
369.68	5.08	666.0	7.376
369.67	5.04	622.3	3.849
369.67	5.02	578.0	1.425
369.67	5.03	537.2	0.742
369.67	5.03	514.4	0.693
369.67	5.03	494.8	0.826
369.67	5.02	450.4	2.163
369.67	5.01	402.9	5.578
369.67	4.98	364.7	9.578
369.67	4.90	321.6	18.611
369.67	4.75	278.4	30.864
369.67	4.48	231.6	52.802
369.67	4.01	180.8	99.908
372.93	10.01	916.3	43.250
372.99	9.14	894.9	39.849
372.99	7.51	848.4	33.853
372.99	6.41	792.5	26.665
372.99	5.86	744.1	20.213
372.99	5.59	695.8	14.698
372.99	5.44	642.6	9.408
372.99	5.38	598.8	6.557
372.99	5.33	541.4	4.906
372.99	5.32	512.1	4.793
372.99	5.29	471.0	5.588
372.99	5.25	415.2	8.758
372.99	5.16	360.0	15.657
372.99	5.04	312.1	24.372
372.99	4.81	264.1	38.749
372.99	4.48	217.3	61.313
372.99	3.43	134.2	132.220
387.74	11.08	848.5	36.379
387.74	9.93	808.8	34.927
387.74	8.81	761.1	32.281

R22 isotherms			
T $[K]$	p $[MPa]$	ϱ $[kg/m^3]$	$\mathbf{a} \cdot 10^{-9}$ $[m^2/s]$
387.74	8.09	716.6	27.988
387.74	7.59	671.2	24.166
387.74	7.25	622.8	21.396
387.74	6.96	569.8	19.196
387.74	6.75	519.0	18.444
387.74	6.62	482.4	18.855
387.74	6.47	445.0	20.535
387.74	6.28	395.9	24.683
387.74	6.13	365.0	28.717
387.74	5.89	321.8	37.390
387.74	5.57	276.5	48.929
387.74	5.20	234.2	63.998
387.74	4.77	198.2	93.135
387.74	4.34	168.3	125.699
406.23	9.83	636.0	31.525
406.23	9.40	603.3	30.392
406.23	8.96	561.8	29.611
406.23	8.58	520.1	30.242
406.23	8.17	471.5	31.152
406.23	7.77	420.9	34.488
406.23	7.45	382.8	39.123
406.23	6.91	322.9	48.428
406.23	6.55	289.1	55.672
406.23	6.09	249.7	67.944
406.23	5.53	211.1	89.055
406.23	4.80	167.7	115.746
406.23	4.41	124.5	149.946

R22 critical isochore			
T $[K]$	p $[MPa]$	ϱ $[kg/m^3]$	$\mathbf{a} \cdot 10^{-9}$ $[m^2/s]$
369.43	4.99	520.0	0.343
369.49	4.99	520.0	0.481
369.64	5.01	520.0	0.713

R22 critical isochore			
T $[K]$	p $[MPa]$	ϱ $[kg/m^3]$	$\mathbf{a} \cdot 10^{-9}$ $[m^2/s]$
369.80	5.02	520.0	0.951
370.03	5.05	520.0	1.236
370.37	5.08	520.0	1.681
370.87	5.12	520.0	2.339
371.61	5.19	520.0	3.215
372.68	5.30	520.0	4.461
374.27	5.45	520.0	6.182
376.59	5.68	520.0	8.583
380.00	6.02	520.0	11.890
385.01	6.51	520.0	16.266
392.36	7.24	520.0	21.744
403.15	8.31	520.0	28.456

R22 two-phase fluid			
T $[K]$	p $[MPa]$	ϱ $[kg/m^3]$	$\mathbf{a} \cdot 10^{-9}$ $[m^2/s]$
298.15	1.03	1184.0	56.668
303.16	1.18	1165.5	54.393
327.56	2.14	1055.3	45.334
342.96	2.98	967.6	36.231
352.67	3.62	899.2	29.864
358.80	4.07	835.8	23.534
362.67	4.38	787.0	17.901
365.11	4.59	745.0	12.927
366.65	4.73	711.6	9.142
367.61	4.81	683.0	6.434
368.23	4.87	660.2	4.288
368.62	4.91	639.9	2.918
368.86	4.93	623.3	2.011
369.02	4.94	608.4	1.334
369.11	4.95	595.0	0.904
369.18	4.96	584.8	0.616
369.21	4.96	575.8	0.426
369.24	4.96	566.5	0.292

R22 two-phase gas			
T $[K]$	p $[MPa]$	ϱ $[kg/m^3]$	$\mathbf{a} \cdot 10^{-9}$ $[m^2/s]$
316.75	1.66	74.0	187.113
327.56	2.14	94.4	143.038
342.96	2.98	141.1	84.310
352.67	3.61	192.9	53.451
358.80	4.07	240.5	34.612
362.67	4.38	274.6	22.388
365.11	4.59	306.0	14.770
366.65	4.72	339.8	9.814
367.61	4.81	363.5	6.513
368.23	4.87	387.5	4.377
368.62	4.91	407.1	2.933
368.86	4.93	429.5	2.048
369.02	4.94	436.7	1.379
369.11	4.95	447.8	0.953
369.18	4.96	459.2	0.667
369.21	4.96	470.9	0.465
369.24	4.96	474.0	0.305

R134a isotherms			
T $[K]$	p $[MPa]$	ϱ $[kg/m^3]$	$\mathbf{a} \cdot 10^{-9}$ $[m^2/s]$
370.36	10.30	982.8	42.541
370.36	7.72	939.6	37.155
370.36	6.03	896.8	33.610
370.36	4.96	856.1	29.483
370.36	4.39	823.5	24.791
370.36	4.03	788.6	20.993
370.36	3.82	755.0	16.336
370.36	3.70	276.4	22.247
370.36	3.56	234.0	42.625
370.36	3.33	192.9	64.869
370.36	3.09	164.9	87.419
370.36	2.65	125.2	188.524
373.72	8.28	930.4	41.534

R134a isotherms			
T $[K]$	p $[MPa]$	ϱ $[kg/m^3]$	$\mathbf{a} \cdot 10^{-9}$ $[m^2/s]$
373.72	6.73	893.9	34.216
373.72	5.53	846.8	30.706
373.72	4.89	810.9	26.011
373.72	4.37	761.9	20.207
373.72	4.14	719.1	14.505
373.72	4.03	672.2	8.479
373.72	4.00	629.8	3.762
373.72	3.98	369.1	6.526
373.72	3.94	324.7	15.028
373.72	3.89	297.3	21.973
373.72	3.78	259.4	34.263
373.72	3.52	206.0	60.389
373.72	3.19	166.8	90.413
373.72	2.60	118.2	208.655
374.47	10.40	965.3	33.222
374.47	7.79	916.1	30.491
374.47	6.03	861.6	26.706
374.47	4.93	804.7	23.829
374.47	4.40	750.2	18.635
374.47	4.17	698.9	12.506
374.47	4.09	646.1	6.630
374.47	4.06	595.4	2.426
374.47	4.05	544.5	0.958
374.47	4.05	518.4	0.758
374.47	4.06	500.8	0.761
374.47	4.05	455.2	1.540
374.47	4.04	411.8	3.592
374.47	4.03	375.1	7.364
374.47	3.99	333.1	14.457
374.47	3.88	284.6	27.228
374.47	3.70	238.9	42.882
374.47	3.25	173.8	76.195
374.47	2.16	91.0	283.867
377.84	4.60	697.2	15.450
377.84	4.51	678.7	12.093
377.84	4.45	634.3	10.252
377.84	4.40	596.6	7.599
377.84	4.37	564.9	6.274

R134a isotherms			
T $[K]$	p $[MPa]$	ϱ $[kg/m^3]$	$\mathbf{a} \cdot 10^{-9}$ $[m^2/s]$
377.84	4.35	529.8	5.321
377.84	4.34	516.7	5.130
377.84	4.33	503.7	5.169
377.84	4.31	468.4	5.528
377.84	4.30	433.0	7.089
377.84	4.25	383.7	11.310
377.84	4.20	349.2	16.275
377.84	4.10	301.4	25.546
377.84	3.94	259.8	36.614
377.84	3.80	233.1	47.838
392.79	8.41	806.2	32.963
392.79	7.20	740.6	27.264
392.79	6.46	677.2	23.488
392.79	6.02	609.1	21.354
392.79	5.81	563.8	20.210
392.79	5.64	521.1	19.538
392.79	5.52	486.1	19.939
392.79	5.40	448.0	21.252
392.79	5.17	389.5	26.508
392.79	4.95	331.7	34.435
392.79	4.65	276.7	47.669
392.79	4.22	225.2	73.874
392.79	3.59	165.4	104.510
411.51	10.00	719.1	42.142
411.51	9.67	701.7	39.964
411.51	9.04	670.1	38.405
411.51	8.52	633.3	36.238
411.51	8.11	597.3	34.522
411.51	7.69	553.2	32.783
411.51	7.36	515.1	32.522
411.51	7.06	480.9	33.468
411.51	6.72	433.2	36.238
411.51	6.45	398.1	39.243
411.51	6.07	347.0	49.085
411.51	5.68	301.2	58.095
411.51	5.13	249.0	73.491
411.51	4.48	196.0	98.987

R134a critical isochore			
T $[K]$	p $[MPa]$	ϱ $[kg/m^3]$	$\mathbf{a} \cdot 10^{-9}$ $[m^2/s]$
374.14	4.03	512.2	0.186
374.22	4.04	512.2	0.357
374.38	4.05	512.2	0.617
374.59	4.07	512.2	0.947
374.87	4.09	512.2	1.380
375.33	4.13	512.2	2.022
376.05	4.19	512.2	3.015
377.19	4.28	512.2	4.488
379.00	4.43	512.2	6.699
381.87	4.67	512.2	9.792
386.42	5.05	512.2	14.153
405.04	6.58	512.2	28.154
423.14	8.09	512.2	36.939

R134a two-phase fluid			
T $[K]$	p $[MPa]$	ϱ $[kg/m^3]$	$\mathbf{a} \cdot 10^{-9}$ $[m^2/s]$
303.15	0.79	1189.3	48.603
325.72	1.40	1095.5	41.440
343.92	2.15	993.7	32.492
355.11	2.73	916.1	27.563
362.19	3.17	852.2	24.193
366.66	3.47	797.5	19.730
369.41	3.67	753.6	14.460
371.21	3.80	715.1	10.913
372.34	3.89	682.6	8.229
373.06	3.95	653.4	4.620
373.50	3.98	628.1	2.847
373.79	4.00	603.3	1.618
373.96	4.02	578.5	0.748
374.08	4.03	548.5	0.156

R134a two-phase gas			
T $[K]$	p $[MPa]$	ϱ $[kg/m^3]$	$\mathbf{a} \cdot 10^{-9}$ $[m^2/s]$
343.92	2.15	114.9	140.044
355.11	2.73	163.4	79.920
362.19	3.17	209.9	45.857
366.66	3.47	248.8	28.569
369.41	3.67	284.6	19.059
371.21	3.80	318.1	13.145
372.34	3.89	345.8	7.902
373.06	3.95	372.8	4.750
373.50	3.98	396.3	2.987
373.79	4.00	417.5	1.760
373.96	4.02	441.0	0.848
374.08	4.03	472.3	0.194